Journal of Power Sources 209 (2012) 152–157

Contents lists available at SciVerse ScienceDirect

Journal of Power Sources

journal homepage: www.elsevier.com/locate/jpowsour

A self-template synthesis of hierarchical porous carbon foams based on banana peel for supercapacitor electrodes

Yaokang Lv[a], Lihua Gan[a,*], Mingxian Liu[a], Wei Xiong[a], Zijie Xu[a], Dazhang Zhu[a], Dominic S. Wright[b]

[a] Department of Chemistry, Tongji University, 1239 Siping Road, Shanghai 200092, PR China
[b] Department of Chemistry, University of Cambridge, Lensfield Road, Cambridge CB2 1EW, UK

ARTICLE INFO

Article history:
Received 28 December 2011
Received in revised form 10 February 2012
Accepted 22 February 2012
Available online 3 March 2012

Keywords:
Hierarchical porous carbon foams
Synthesis
Banana peel
Electrochemical properties
Supercapacitor

ABSTRACT

Hierarchical porous carbon foams (denoted as HPCFs) is prepared through a novel self-template strategy based on banana peel. Banana peel, which contains natural porous structure formed by biopolymers in cell walls, can absorb ions and phenolic compounds. The carboxylic and hydroxyl groups on the pores' surface will coordinate with zinc ions to form zinc complexes. These zinc complexes which are similar with metal–organic frameworks are used as self-template, and the aminophenol furfural resin polymerized in the pores of complexes is used as the additional carbon source to create hierarchical porous structure during the carbonization process. The resulted HPCFs are composed of macroporous cores with mesoporous and microporous channels. The unique self-supported hierarchical structure possesses a high specific surface area ($1650\,m^2\,g^{-1}$) and provides a more favorable path for electrolyte penetration and transportation, which give rise to the excellent electrochemical property of HPCFs as an electrode material for supercapacitor. The calculated specific capacitance of HPCFs electrode in $6\,mol\,L^{-1}$ KOH is $206\,F\,g^{-1}$ at a current density of $1\,A\,g^{-1}$, while the specific capacitance still exhibits relative high ($182\,F\,g^{-1}$) at a higher current density of $10\,A\,g^{-1}$ with the retention of 88%.

1. Introduction

Porous carbon materials represent very attractive materials for use as catalyst supports [1,2], adsorbents [3], and electrode materials [4–8]. Extensive methods [9–15] including laser ablation [9], electrical arc [10], chemical-vapor decomposition [11], nanocasting [12,13], and chemical or physical activation [14] have been employed to prepare various carbon materials for different applications. As advanced electrode materials for supercapacitors, it is desirable to structure the porous carbon with pores of multi-scales. Ion-buffering reservoirs formed in the macropores to minimize the diffusion distances to the interior surfaces [6]. The mesoporous channels provide low-resistant pathways for the ions through the porous particles [7], and the micropores strengthen the electric-double-layer capacitance [8]. Therefore optimum pore structures are supposed to possess smaller pores interconnected with larger sets of pores, which could achieve high surface area and efficient ion diffusion pathways simultaneously. Among these reported carbon materials, hierarchical porous carbons have been proposed to yield good specific energy density and power density [5].

Recent research [16–20] has shown that several metal–organic coordination polymers or metal–organic frameworks (MOFs) such as $Zn_4O(OOCC_6H_4COO)_3$ (MOF-5) [16,20] can be used as the templates or precursors for the preparation of porous carbon with high surface area. In 2008, Liu et al. [16] firstly reported the use of MOF-5 as a template for preparing nanoporous carbon, which exhibits high surface area and excellent electrochemical performance as an electrode material. In 2010, Hu et al. [20] prepared porous carbon for supercapacitors through the direct thermolysis of MOF-5 with or without phenolic resin or carbon tetrachloride and ethylenediamine as the additional carbon sources. They found that different carbon sources can result in different pore structures. In 2011, Radhakrishnan et al. [19] demonstrated the preparation of microporous carbon fibers through carbonization of Al-based MOFs with furfuryl alcohol under an inert gas atmosphere. Interestingly, the fibrous morphology of the original MOFs is successfully retained after the carbonization process. However, in order to obtain specific MOFs, pure reagents and the strict control of reaction conditions are required [21,22]. Therefore these reported synthetic procedures for porous carbon are still complicated and the preparation costs are relatively high.

On the other hand, many natural materials are generally abundant, renewable, inexpensive and environmentally benign compared to artificial templates and precursors. Using natural biological components to construct carbon materials has received extensive attention [23–25]. Growing high-quality carbon materials from these low-valued carbon sources opens an effective way to convert the waste carbon sources into a high-value-added product.

* Corresponding author. Tel.: +86 21 65982654 8430; fax: +86 21 65981097.
E-mail address: ganlh@tongji.edu.cn (L. Gan).

0378-7753/$ – see front matter © 2012 Elsevier B.V. All rights reserved.
doi:10.1016/j.jpowsour.2012.02.089

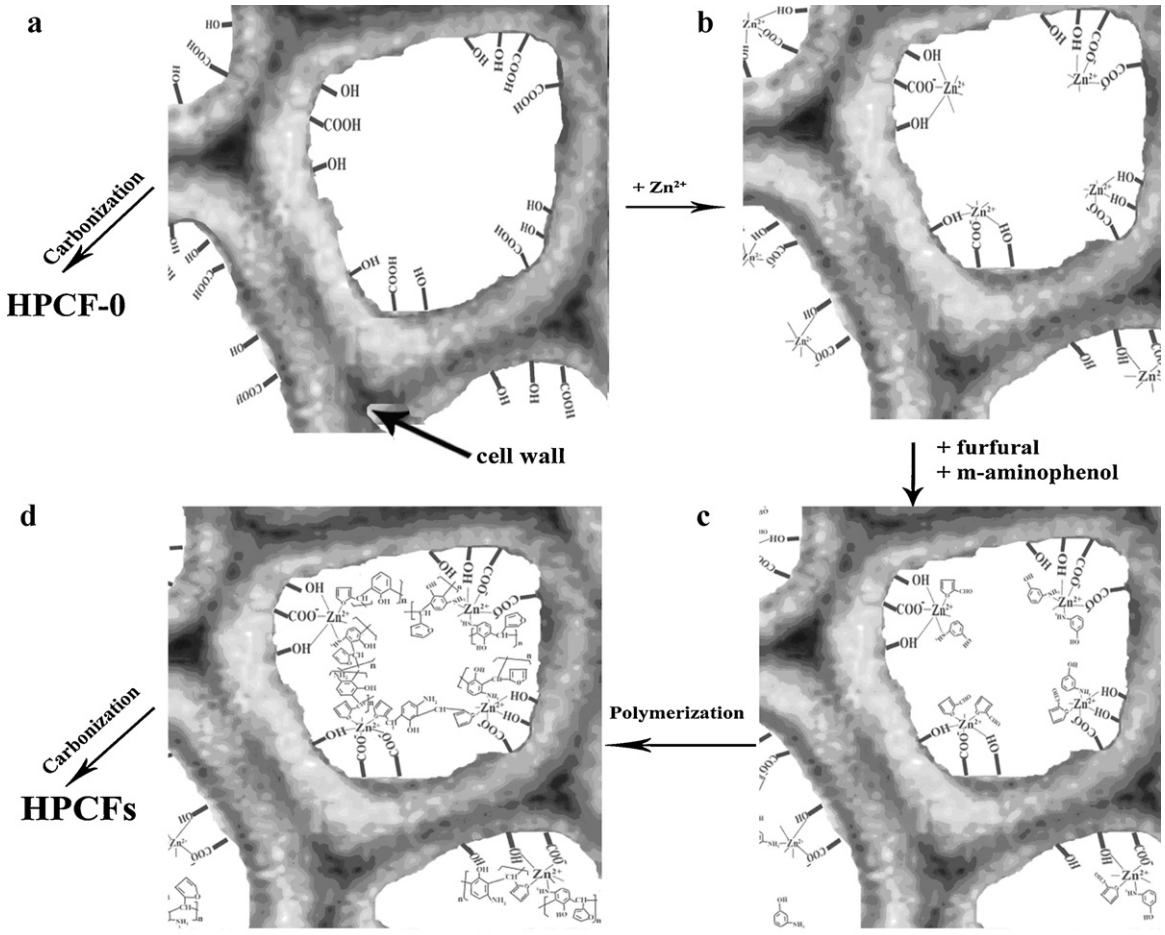

Fig. 1. Schematic illustration of the formation process of HPCFs and HPCF-0.

Banana peel, a common agricultural waste, represents 40% of the total weight of fresh banana. The texture of banana peel contains abundant porous structure which is formed by biopolymers in plant cell walls such as celluloses, hemicelluloses, pectins, lignins and proteins [26]. Some investigations had reported that banana peel is an economical and selective sorbent for the adsorption of phenolic compounds as well as heavy metal ions such as Cu(II), Ni(II), Cr(IV), Cd(II), and Pb(II) from aqueous solution not only due to their pore structures but also attributed to the carboxyl and hydroxyl groups on the surface of pores, which can easily bind to metal ions to remove metal ions from solution [27–33]. Recently, banana peel extract was used for the synthesis of palladium nanoparticles and silver nanoparticles [32,33].

Herein, we report a novel self-template strategy for the synthesis of hierarchical porous carbon foams (denoted as HPCFs) based on banana peel. The carboxylic groups and hydroxyl groups on the pores' surface of banana peel could coordinate with zinc ions to form zinc complexes which are similar with metal–organic frameworks. This banana peel based zinc complexes were used as the self-template, and the aminophenol furfural resin polymerized in the pores of complexes was used as the additional carbon source to prepare HPCFs. The obtained HPCFs possess high surface area with a well designed 3D interconnected porous texture combining macroporous cores, mesoporous channels and micropores, which give rise to excellent performances as an electrode material for supercapacitor. Besides, owing to its ease and low cost of production, this self-template approach would be industrially feasible. Therefore, the present finding provides the promising prospects for the application of HPCFs as electrode materials in supercapacitors.

2. Experimental

2.1. Syntheses of HPCFs

The formation process of the HPCFs is based on a simple and reproducible pathway (Fig. 1). In a typical procedure, firstly, the collected biomaterial was extensively washed under water, cut into small pieces (Fig. 1a), and then marinated in 2 mol L^{-1} zinc nitrate solution for a week at 70 °C. The absorbed zinc ions were coordinated with the carboxylic groups and hydroxyl groups on the surface of banana peel and the brown zinc complexes (Fig. 1b) were obtained after drying at 60 °C. Secondly, the zinc complexes were further suspended in a solution containing furfural and 2-aminophenol for a week at 70 °C, the resultant material was dried and subsequently cured at 120 °C. In the process, the furfural and 2-aminophenol molecules entered the natural pores of the zinc complexes (Fig. 1c), then they were polymerized together in the pores and co-assembled into a composite of the aminophenol furfural resin-zinc complexes (composite 1) (Fig. 1d). Finally, the carbonization of composite 1 was performed at 1000 °C for 8 h under N_2 atmosphere to obtain HPCFs. As a comparison, we synthesized another carbon material (denoted as HPCF-0) through direct carbonization of banana peel.

2.2. Characterization

Infrared (IR) spectra were measured in KBr pellets on a Nicolet 5DX FT-IR spectrometer. Elemental analyses were performed on a Perkin-Elmer 2400II elemental analyzer. Thermal gravimetric

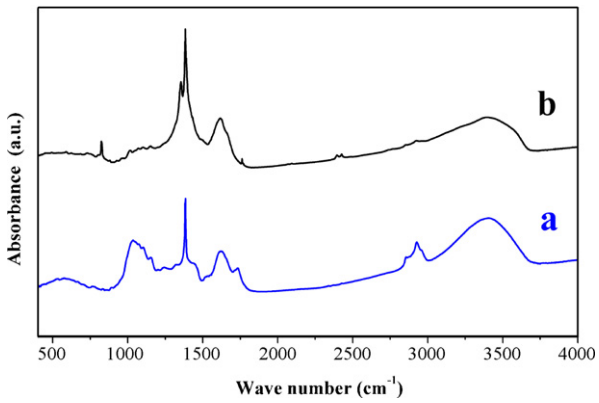

Fig. 2. IR spectra of dried banana peel (a) and composite 1 (b) obtained with 1 mg of adsorbent and 500 mg of KBr.

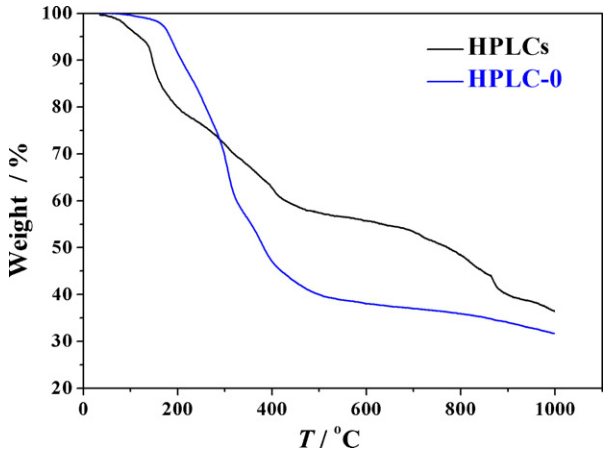

Fig. 3. TG curves of dried banana peel (a) and composite 1 (b) used in this work at a heating rate of 10 °C min^{-1} with a nitrogen flow.

(TG) analysis was carried out using a Netzsch STA 449C thermoanalysis instrument in the temperature range of 30–1000 °C with a heating rate of 5 K min^{-1} under nitrogen atmosphere. Powder X-ray diffraction (XRD) experiments were taken on a Bruker D8 Advance diffractometer with Cu Kα (λ = 0.154056 Å) radiation. Raman spectra were obtained by using a Renishaw Invia system, under λ_{exc} = 514 nm laser excitation. Nitrogen adsorption/desorption isotherms were measured at the liquid nitrogen temperature using a Micromeritics Tristar 3000 analyzer. Scanning electron microscopy (SEM) image was obtained by using Philips XL-30 SEM. Transmission electron microscopic (TEM) observations were conducted on a JEOL2100 microscope operated at 200 kV.

2.3. Electrochemical evaluation

The electrochemical measurements were done in a conventional three-electrode experimental setup [34–36]. The electrolyte was a 7 mol L^{-1} KOH aqueous solution. Saturated calomel electrode (SCE) was used as reference electrode, and nickel foams as the counter-electrode. The working electrode was prepared without adding any conductive agents. The powder of HPCFs were mixed with polytetrafluoroethylene with a mass ratio of 9:1. The mixture was pressed between two pieces of nickel foam under 30 MPa. Thereafter, the 0.50 mm thick electrode was dried overnight at 100 °C. Cyclic voltammograms and galvanostatic charge–discharge behavior were tested in electrolyte of 6 mol L^{-1} KOH using CHI 660D electrochemical workstation, and the potential window was chosen in the range of −1.0 to 0 V versus SCE. The specific capacitances calculated from the CV curves are based on the following equation: $C_s = (I/m)/(dE/dt)$, where I is the current at −0.50 V, dE/dt is the scan rate, and m is the mass of active material. The specific capacitance calculated from galvanostatic charge–discharge cycling experiments are calculated by the equation of $C_g = i\Delta t/(\Delta V m)$, where i is the constant discharging current, Δt is the discharge time, ΔV is the voltage window from the end of the ohmic drop to the end of the discharge process, and m is the mass of active materials on single electrode.

3. Results and discussion

IR spectra of dried banana peel (a) and composite 1 (b) are shown in Fig. 2. The spectra of dried banana peel (Fig. 2a) displayed a number of peaks. Adsorption bands appearing at 3403.8, 2927.5, 2856.1, 1733.7, 1623.8, 1384.7, 1035.6 and 891.0 cm^{-1} in Fig. 2a were assigned to O—H stretching, C—H stretching of alkane, C—H and C=O stretching of carboxylic acid or ester, COO^- anion stretching, O—H bending, C—O stretching of ester or ether and N—H deformation of amines respectively [37]. Fig. 2b shows the FT-IR spectrum of composite 1. As expected, compared with that of dried banana peel (Fig. 2a), the prominent peak intensity of carboxylic groups and hydroxyl groups at 3403, 2928, 1734, 1624 and 1036 cm^{-1} was significantly reduced, confirming the coordination linkage of carboxylic acid and hydroxyl groups with zinc ions. Besides, there are several new weak absorbed peaks appearing at 827, 733 and 687 cm^{-1} which were attributed to the vibrations of the aromatic compounds, and a new peak founded at 1356 cm^{-1} should be attributed to the anti-symmetric stretching vibrations of nitrate. It has been reported that banana peel can be used as biosorbent for adsorbing phenolic compounds [28] and metal ions. The carboxyl groups and hydroxyl groups of banana peel can form coordination linkages with metal ions [27,38]. These results indicate that banana peel was coordinated with zinc ions and adsorbed furfural and 2-aminophenol which further co-assemble into composite 1 after polymerization.

When being subjected to thermal treatment with a N_2 flow, the zinc complexes in composite 1 acted as the template was transformed into the ZnO/carbon composites at 550 °C, At temperatures higher than 800 °C, ZnO was reduced into metallic zinc [16,39] during the carbonization process, and at 1000 °C, metallic zinc was vaporized in the N_2 flow, leaving carbon species alone in the resulting HPCFs sample. As shown in Fig. 3, the TG curves of dried banana peel and composite 1 indicated that the rate of residual carbon of composite 1 was 36.4%, more than that of dried banana peel (31.6%).

C, H and N elemental analysis show that as-synthesized HPCFs contains 87.4 wt.% of carbon, 1.6 wt.% of hydrogen, and 4.3 wt.% of nitrogen, while HPCF-0 contains 86.2 wt.% of carbon, 2.1 wt.% of hydrogen, and 0.6 wt.% of nitrogen. It is clearly demonstrated that N incorporates into the framework of HPCFs. It was reported that increasing the nitrogen content of carbon materials could enhance their graphitization degree [40,41], and consequently improve their electrical conductivity. As shown in Fig. 4, the XRD pattern for HPCFs displays two broad peaks at 2θ = 25 and 44°, corresponding to the (0 0 2) and (1 0 0) diffractions for carbon. No diffractions were observed for Zn species in HPCFs. However, there was no significant peak in the XRD pattern of HPCF-0, indicating its amorphous state. The empirical parameter (R) was used to evaluate the degree of graphitization, which is defined as the ratio of height of the (0 0 2) Bragg peak to the background [42,43], Therefore the degree of graphitization of HPCFs is higher than that of HPCF-0. The Raman spectra of HPCF-0 and HPCFs are displayed in Fig. 5. Both the spectra show a distinct pair of broad bands around 1580 (G band) and 1340 cm^{-1} (D band). The G band and D band are assigned to the hexagonal carbon plane and crystal defects or imperfections, respectively. The ratio of the relative intensity of these two bands

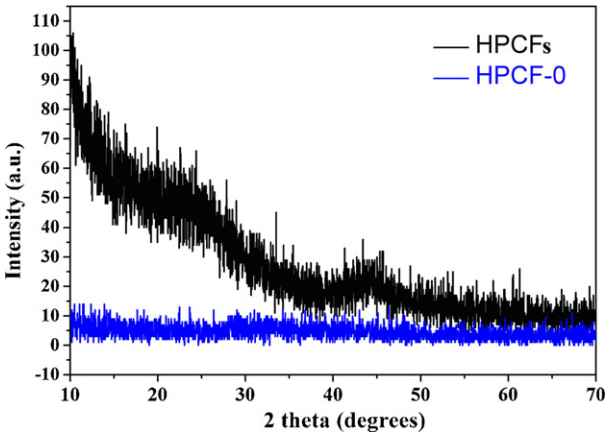

Fig. 4. XRD patterns of the resultant porous carbons foams: HPCF-0 and HPCFs.

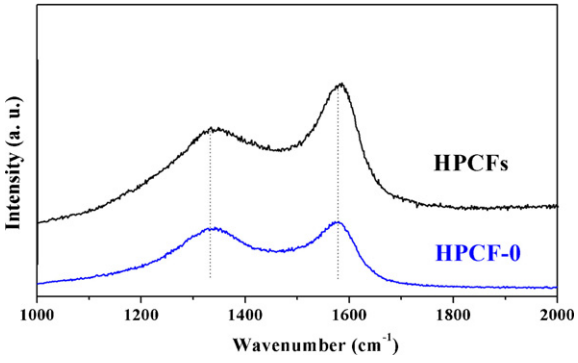

Fig. 5. Raman spectra of HPCF-0 and HPCFs.

(I_D/I_G) is proportional to the number of defect sites in the graphite carbon. The lower the ratio is, the higher the graphitization is [4]. It can be calculated that the I_D/I_G ratio of HPCF-0 is 0.93 and that of HPCFs is 0.76. The result confirmed that HPCFs has much higher graphitization degree and consequent higher conductivity in comparison with HPCF-0.

As shown in Fig. 6a, the Type-IV [44] nitrogen sorption isotherms for HPCFs suggest the existence of different pore sizes from micro- to macropores. The steep increase in the adsorbed volume at low relative pressure is related with the presence of micropores, the desorption hysteresis at medium relative pressure reveals the existence of developed mesopores, and the almost vertical tails at a relative pressure near to 1.0 denotes the presence of macroporosity. Therefore, the hierarchical pore structure of HPCFs is composed of micropores, mesopores and macropores. The Brunauer–Emmett–Teller (BET) surface area of HPCFs is 1650 $m^2 g^{-1}$ with the total pore volume of 1.26 cm^3 as well as the average pore size width of 3.01 nm. In contrast, the nitrogen sorption isotherm is an approximately typical Type-I for HPCF-0, indicating its apparent micropore characteristic. The BET surface area of HPCF-0 is only 131 $m^2 g^{-1}$. The pore size distributions of HPCFs and HPCF-0 calculated from the nitrogen desorption branches by Barrett–Joyner–Halenda analysis are given in Fig. 6b. HPCFs display typical hierarchical pore size distribution with a highest peak centering at ca. 3.6 nm, as well as several lower peaks centering at ca. 1.8, 2.8 and 16.4 nm. It can be clearly observed that the majority of pores of HPCFs are located in the region of mesopores. In comparison, the pore sizes of HPCF-0 are located in the region of micropores.

More structural details were investigated by SEM (Fig. 7) and TEM (Fig. 8) observations. Fig. 7a shows the texture of the macroporous cores of HPCF-0, the sizes of most pores are larger than

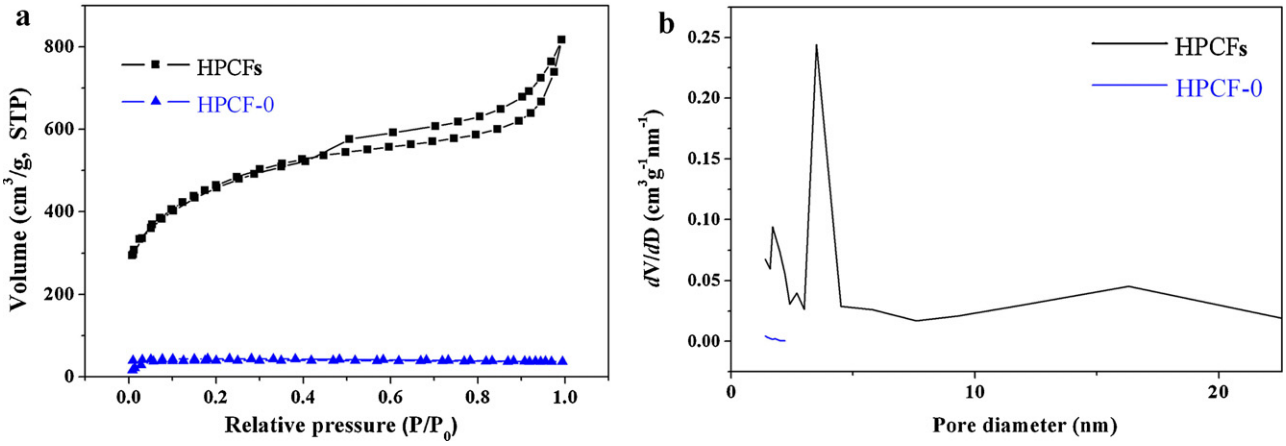

Fig. 6. Nitrogen adsorption–desorption isotherms (a) and pore size distributions calculated from N_2 desorption isotherms (b) for HPCF-0 and HPCFs.

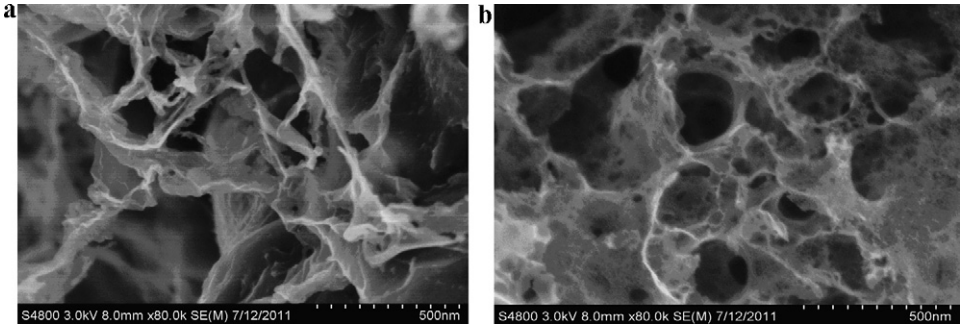

Fig. 7. SEM images of HPCF-0 (a) and HPCFs (b).

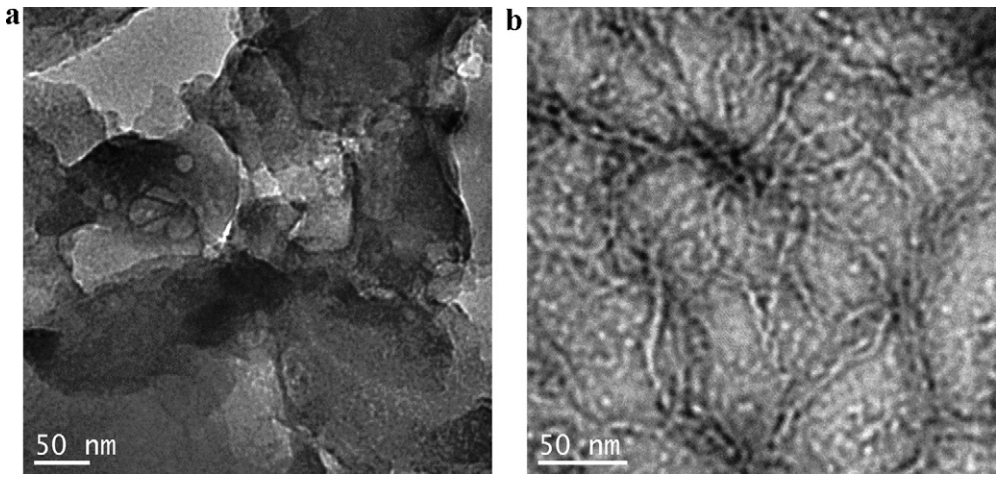

Fig. 8. TEM images of HPCF-0 (a) and HPCFs (b).

100 nm, and the thickness of the walls around them is less than 10 nm. It can be seen that HPCF-0 has uninterrupted network and open structure constructed with nano carbon fibers from the carbonization of biopolymers of banana peel, and there are a few natural micro cracks retained on the pore walls (Fig. 8a). HPCFs also has an open structure with interconnected macropores but there are many new pores smaller than 50 nm on the walls of macroporous cores (Fig. 7b), which affect its electrochemical performance. The TEM image (Fig. 8b) reveals that the sizes of natural cracks in HPCFs are expanded and there are lots of new disorder mesoporous and microporous texture on the pore walls which can provide a short ion-transport pathway through the walls. Hence, HPCFs will have good electrochemical properties due to its high surface area and self-supported hierarchical structure composed of macroporous cores with mesoporous and microporous channels.

The improved graphitization degree and the hierarchical structure of HPCFs are expected to enhance its electrochemical properties [45]. Fig. 9 shows the cyclic voltammetry curves of HPCFs electrodes, whose potential window was chosen in the range of −1 to 0 V versus SCE. It can be observed that the HPCFs electrode presents a nearly perfect quasi-rectangular voltammogram shape at sweep rates from 20 to 400 mV s^{-1} without any redox peaks. During the electrochemical tests, three electrochemical processes are involved, buffering ions in the macroporous cores, transporting ions through the mesoporous channels, and confining ions in the micropores. At high sweep rates, the specific capacitance is mostly attributed to mesopores and macropores of HPCFs. The specific capacitance decays ca. 15% with the increasing sweep rates from

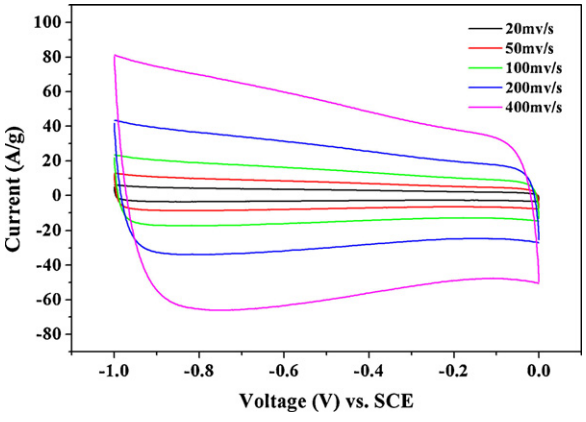

Fig. 9. Cyclic voltammetry curves of HPCFs at different loading current densities.

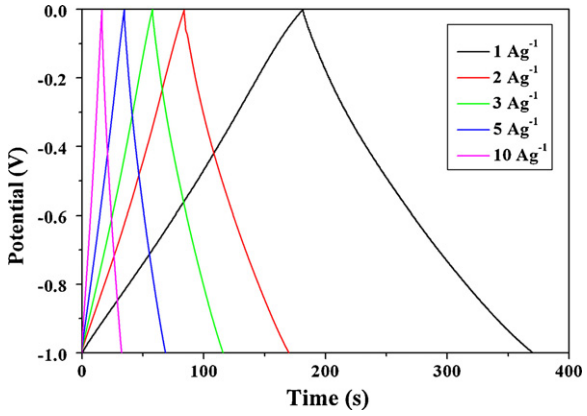

Fig. 10. Galvanostatic charge–discharge curves of HPCFs at different scanning rates.

20 to 400 mV s^{-1} (Fig. S1), indicating the excellent mesoporosity and consequent good capacitance retention of HPCFs.

The galvanostatic charge–discharge behaviors at various current densities are also measured for specific capacitance evaluation. As shown in Fig. 10, no obvious voltage drop can be observed at the beginning of the discharge process for the HPCFs electrode, and the charge–discharge curves at current densities from 1 A g^{-1} to 10 A g^{-1} display regularly triangular shapes showing good columbic efficiency and ideal capacitor behavior for HPCFs. As shown in Fig. S2, with the current increases, the capacitance of HPCFs declined slightly. The calculated specific capacitance of HPCFs is 206 F g^{-1} at a current density of 1 A g^{-1}, while the specific capacitance still exhibits relative high (182 F g^{-1}) at a higher current density of 10 A g^{-1} with the retention of 88%. These results indicate that HPCFs is suitable for fast ion transportation. As an electrode material for supercapacitors, HPCFs exhibits excellent electrochemical performance especially at high current density. Fig. S3 displays the variations in discharge capacitance for the HPCFs electrode as a function of cycle number at a current density of 10 A g^{-1}. It is noteworthy that HPCFs electrode exhibited about 1.7% capacitance decay after 1000 cycles.

4. Conclusions

We have for the first time employed banana peel based zinc complexes as a self-template to prepare HPCFs. The resulted HPCFs are composed of macroporous cores with mesoporous and microporous channels. The unique self-supported hierarchical structure

possesses a high specific surface area (1650 $m^2\,g^{-1}$) and provides a more favorable path for electrolyte penetration and transportation, which give rise to the excellent electrochemical property of HPCFs as an electrode material for supercapacitor. The calculated specific capacitance of HPCFs electrode in 6 mol L^{-1} KOH is 206 $F\,g^{-1}$ at a current density of 1 $A\,g^{-1}$, while the specific capacitance still exhibits relative high (182 $F\,g^{-1}$) at a higher current density of 10 $A\,g^{-1}$ with the retention of 88%, and it is noteworthy that HPCFs electrode operated at a current density of 10 $A\,g^{-1}$ exhibited about 1.7% capacitance decay after 1000 cycles. Besides, this self-template approach would be industrially feasible due to its ease and low cost of production. The results demonstrated in this work offer the promising prospects for the application of HPCFs with high current charge and discharge capability as electrode materials in supercapacitors which meet the need of high power density.

Acknowledgements

The project was supported by the National Natural Science Foundation of China (No. 20973127), Shanghai Nanotechnology Promotion Center (No. 11nm0501000) and the Fundamental Research Funds for the Central Universities (No. 2011KJ023).

Appendix A. Supplementary data

Supplementary data associated with this article can be found, in the online version, at doi:10.1016/j.jpowsour.2012.02.089.

References

[1] H. Suda, K. Haraya, Chem. Commun. (1997) 93–94.
[2] L.F. Velasco, B. Tsyntsarski, B. Petrova, T. Budinova, N. Petrov, J.B. Parra, C.O. Ania, J. Hazard. Mater. 184 (2010) 843–848.
[3] F. Rodriguez-Reinoso, Carbon 36 (1998) 159–175.
[4] Y. Lv, M. Liu, L. Gan, Y. Cao, L. Chen, W. Xiong, Z. Xu, Z. Hao, H. Liu, L. Chen, Chem. Lett. 40 (2011) 236–238.
[5] D.W. Wang, F. Li, M. Liu, G.Q. Lu, H.M. Cheng, Angew. Chem. Int. Ed. 47 (2008) 373–376.
[6] D.R. Rolison, Science 299 (2003) 1698–1701.
[7] T. Morishita, Y. Soneda, T. Tsumura, M. Inagaki, Carbon 44 (2006) 2360–2367.
[8] J. Chmiola, G. Yushin, Y. Gogotsi, C. Portet, P. Simon, P.L. Taberna, Science 313 (2006) 1760–1763.
[9] A. Thess, R. Lee, P. Nikolaev, H.J. Dai, P. Petit, J. Robert, C.H. Xu, Y.H. Lee, S.G. Kim, A.G. Rinzler, D.T. Colbert, G.E. Scuseria, D. Tomanek, J.E. Fischer, R.E. Smalley, Science 273 (1996) 483–487.
[10] C. Journet, W.K. Maser, P. Bernier, A. Loiseau, M.L. Delachapelle, S. Lefrant, P. Deniard, R. Lee, J.E. Fischer, Nature 402 (1999) 276–279.
[11] B. Zheng, C.G. Lu, G. Gu, A. Makarovski, G. Finkelstein, J. Liu, Nano Lett. 2 (2002) 895–898.
[12] M. Liu, L. Gan, C. Tian, J. Zhu, Z. Xu, Z. Hao, L. Chen, Carbon 45 (2007) 3045–3046.
[13] T.W. Kim, I.S. Park, R. Ryoo, Angew. Chem. Int. Ed. 42 (2003) 4375–4379.
[14] B. Xu, F. Wu, R. Chen, G. Cao, S. Chen, Y. Yang, J. Power Sources 195 (2010) 2118–2124.
[15] Y.I. Jang, N.J. Dudney, T.N. Tiegs, J.W. Klett, J. Power Sources 161 (2006) 1392–1399.
[16] B. Liu, H. Shioyama, T. Akita, Q. Xu, J. Am. Chem. Soc. 130 (2008) 5390–5391.
[17] M. Hu, J. Reboul, S. Furukawa, L. Radhakrishnan, Y.J. Zhang, P. Srinivasu, H. Iwai, H.J. Wang, Y. Nemoto, N. Suzuki, S. Kitagawa, Y. Yamauchi, Chem. Commun. 47 (2011) 8124–8126.
[18] B. Liu, H. Shioyama, H.L. Jiang, X.B. Zhang, Q. Xu, Carbon 48 (2010) 456–463.
[19] L. Radhakrishnan, J. Reboul, S. Furukawa, P. Srinivasu, S. Kitagawa, Y. Yamauchi, Chem. Mater. 23 (2011) 1225–1231.
[20] J.A. Hu, H.L. Wang, Q.M. Gao, H.L. Guo, Carbon 48 (2010) 3599–3606.
[21] H. Li, M. Eddaoudi, M. O'Keeffe, O.M. Yaghi, Nature 402 (1999) 276–279.
[22] A. Carton, A. Mesbah, L. Aranda, P. Rabu, M. Francois, Solid State Sci. 11 (2009) 818–823.
[23] H.J. Liu, X.M. Wang, W.J. Cui, Y.Q. Dou, D.Y. Zhao, Y.Y. Xia, J. Mater. Chem. 20 (2010) 4223–4230.
[24] E. Raymundo-Pinero, F. Leroux, F. Beguin, Adv. Mater. 18 (2006) 1877–1882.
[25] G.D. Ruan, Z.Z. Sun, Z.W. Peng, J.M. Tour, ACS Nano 5 (2011) 7601–7607.
[26] T.H. Emaga, C. Robert, S.N. Ronkart, B. Wathelet, M. Paquot, Bioresour. Technol. 99 (2008) 4346–4354.
[27] M. Thirumavalavan, Y.L. Lai, L.C. Lin, J.F. Lee, J. Chem. Eng. Data 55 (2010) 1186–1192.
[28] M. Achak, A. Hafidi, N. Ouazzani, S. Sayadi, L. Mandi, J. Hazard. Mater. 166 (2009) 117–125.
[29] V.N. Gunaseelan, Bioresour. Technol. 98 (2007) 1270–1277.
[30] A. Bankar, B. Joshi, A.R. Kumar, S. Zinjarde, Colloids Surf. B 80 (2010) 45–50.
[31] R.S.D. Castro, L. Caetano, G. Ferreira, P.M. Padilha, M.J. Saeki, L.F. Zara, M.A.U. Martines, G.R. Castro, Ind. Eng. Chem. Res. 50 (2011) 3446–3451.
[32] A. Bankar, B. Joshi, A.R. Kumar, S. Zinjarde, Mater. Lett. 64 (2010) 1951–1953.
[33] A. Bankar, B. Joshi, A.R. Kumar, S. Zinjarde, Colloids Surf. A 368 (2010) 58–63.
[34] T. Brezesinski, J. Wang, J. Polleux, B. Dunn, S.H. Tolbert, J. Am. Chem. Soc. 131 (5) (2009) 1802–1809.
[35] H. Itai, H. Nishihara, T. Kogure, T. Kyotani, J. Am. Chem. Soc. 133 (5) (2011) 1165–1167.
[36] Q. Lu, M.W. Lattanzi, Y. Chen, X. Kou, W. Li, X. Fan, K.M. Unruh, J.G. Chen, J.Q. Xiao, Angew. Chem. Int. Ed. 50 (30) (2011) 6847–6850.
[37] G. Socrates, Infrared Characteristic Group Frequencies; Tables and Charts, 2nd ed., John Wiley & Sons, 1994.
[38] J.R. Memon, S.Q. Memon, M.I. Bhanger, A. El-Turki, K.R. Hallam, G.C. Allen, Colloids Surf. B 70 (2009) 232–237.
[39] E.A. Fletcher, Ind. Eng. Chem. Res. 38 (1999) 2275–2282.
[40] C.M. Feng, H.X. Li, Y. Wan, J. Nanosci. Nanotechnol. 9 (2009) 1558–1563.
[41] N.D. Kim, W. Kim, J.B. Joo, S. Oh, P. Kim, Y. Kim, J. Yi, J. Power Sources 180 (2008) 671–675.
[42] Y.H. Liu, J.S. Xue, T. Zheng, J.R. Dahn, Carbon 34 (1996) 193–200.
[43] D.Y. Qu, Chem. Eur. J. 14 (2008) 1040–1046.
[44] S. Brunauer, L.S. Deming, W.E. Deming, E. Teller, J. Am. Chem. Soc. 62 (1940) 1723–1732.
[45] Q. Li, R.R. Jiang, Y.Q. Dou, Z.X. Wu, T. Huang, D. Feng, J.P. Yang, A.S. Yu, D.Y. Zhao, Carbon 49 (2011) 1248–1257.